Article

Lithium Niobate Perovskite as the Support for Silver Nanoparticles for Non-Enzymatic Electrochemical Detection of Glucose

Claudia Ivone Piñón-Balderrama [1,2,*] , Atenea Manríquez-Tristán [3], María Cristina Maldonado-Orozco [3] , Claudia Alejandra Hernández-Escobar [2], Simón Yobanny Reyes-López [4] , León Francisco Espinosa-Cristobal [4] and Erasto Armando Zaragoza-Contreras [2,*]

1   CONAHCYT-CIMAV, Miguel de Cervantes No. 120, Complejo Industrial Chihuahua, Chihuahua 31136, Chihuahua, Mexico
2   Centro de Investigación en Materiales Avanzados, S.C. Miguel de Cervantes No. 120, Complejo Industrial, Chihuahua 31136, Chihuahua, Mexico; claudia.hernandez@cimav.edu.mx
3   Faculty of Engineering, Universidad Autónoma de Chihuahua, Circuito Número I s/n, Nuevo Campus Universitario, Nte. 2, Chihuahua 31125, Chihuahua, Mexico; amanriquez@lasallechihuahua.edu.mx (A.M.-T.); cmaldona@uach.mx (M.C.M.-O.)
4   Institute of Biomedical Sciences, Universidad Autónoma de Ciudad Juárez, Envolvente del PRONAF and Estocolmo s/n, Ciudad Juárez 32310, Chihuahua, Mexico; simon.reyes@uacj.mx (S.Y.R.-L.); leon.espinosa@uacj.mx (L.F.E.-C.)
*   Correspondence: claudia.pinon@cimav.edu.mx (C.I.P.-B.); armando.zaragoza@cimav.edu.mx (E.A.Z.-C.)

Abstract: Lithium niobate perovskite and silver nanoparticle-based nanocomposites (LNB:AgNPs) were explored for developing an electrochemical glucose sensor. The perovskite to silver nanoparticle ratios investigated were 4:1, 1:1, 1:2, 2:1, and 1:4. Among these, the 4:1 ratio, with the lowest silver content, demonstrated the most stable performance during glucose quantification via amperometry. The sensor's response was evaluated measuring the current at a fixed potential of 0.7 V following the injection of 1 mM glucose with each addition. The calibration curve obtained from the recorded data exhibited a linear response within the 1 to 15 mM glucose concentration range, achieving a sensitivity of 2 μA/mM, a high correlation coefficient (R^2 = 0.997), and a limit of detection (LOD) of 0.5 μM. The LNB4:1AgNP composite allowed taking advantage of the unique properties of both components in a balanced manner, maximizing the sensor performance in practical applications.

Keywords: electrochemical sensor; glucose; homemade electrode; lithium niobate; perovskite; silver nanoparticles

1. Introduction

Electrochemical sensors, owing to their low cost, fast response speed, low detection limit, ease of use, and versatility, have found extensive utility in various daily life functions like environmental [1], food [2], and biomedical sensing [3]. Therefore, their components, such as the electrode, electrocatalyst, enzymatic system, or support, are constantly being improved. Non-enzymatic electrochemical sensors, in particular, are highly desirable due to their greater stability than enzymatic sensors, which are susceptible to damage caused by various environmental factors [4]. The electrocatalyst plays a crucial role in non-enzymatic electrochemical detection since it is responsible for the oxidation-reduction reactions through electron transfer on the electrode surface and consequently for analyte detection.

Metallic nanoparticles (MNPs), either pure, alloys, or blends, are efficient electrocatalysts that exhibit a high reactivity towards a wide range of analytes, and their electrocatalytic properties can be tailored by manipulating their size and shape [5]. Because of their greater tolerance to environmental and thermal changes, MNPs are more stable than

enzymes; however, they can respond to various substances, limiting their selectivity [6]. Consequently, this poor selectivity is a significant challenge.

Recently, ABO_3-type perovskites have emerged as promising materials for electrocatalysts. The extensive literature on the application of perovskites in electrochemical sensing has highlighted their notable efficiency in detecting various analytes [7]. For instance, thin films of the $LaNiO_{3-x}$ perovskite were used as the support for the immobilization of enzymes (glucose oxidase and creatinase) to detect glucose and creatinine. The electrodes showed high selectivity, excellent sensitivity for both analytes, and wide linear ranges of detection [8]. In another investigation, lanthanum-based perovskites were used as alternatives to noble metal nanomaterial electrocatalysts. In particular, the perovskite $La_{0.6}Sr_{0.4}CoO_{3-\delta}$ demonstrated the greatest electrooxidation towards peroxide and glucose. The electrooxidation activity towards the analytes was related to a synergistic effect between the Co^{+3}/Co^{+4} redox activity and the formation of oxygen vacancies. Furthermore, using reduced oxidized graphite (RGO) improved the detection [9]. On the other hand, the performance of the metal dopant in the Sr_2PdO_3 perovskite in the non-enzymatic electrochemical detection of glucose was studied. Electrochemical studies showed that with a Au doping of 0.3, the electrode presented a greater electrocatalytic activity than with other metals (Ni, Cu, or Pt). The modified electrode showed high sensitivity, stability, and selectivity in the presence of common interferents [10]. In addition, calcium and barium titanate perovskites were used in the non-enzymatic electrochemical sensing of glutamate. Cyclic voltammetry in the presence of glutamate indicated an oxidation peak at 0.6 V. The study also demonstrated that doping with other metals enhances the intensity of the signals. The authors considered the electrocatalytic activity of these perovskites as moderate [11]. Besides the studies mentioned above, the literature concerning other analytes of interest can also be consulted [7,12–14].

Efforts towards perovskite oxide usage have been important; however, the requirement for other complementary materials to enhance the electrocatalytic activity, such as graphenes or carbon nanotubes, has been pointed out [15,16]. Furthermore, authors have also reported that perovskite application as the support material for an electrocatalyst is a promising topic to develop [17]. Supporting materials, such as imprinted polymers, inorganic porous materials, carbon porous materials, and conductive polymers, can significantly improve the performance of the electrocatalysts [18,19]. Due to surface area increase, the dispersion of the electrocatalyst on the electrode surface increases, contributing to the greater electrocatalytic behavior due to the electronic transfer augment.

This work reports lithium niobate (LNB, $LiNbO_3$) perovskite nanofibers, obtained by electrospinning followed by calcination, as the support for silver nanoparticles (AgNPs) to design a non-enzymatic electrochemical glucose sensor. LNB can significantly enhance the performance of AgNPs as an electrocatalyst for glucose oxidation and detection, even at low concentrations.

2. Materials and Methods

2.1. Materials and Reagents

The following materials were used: $AgNO_3$ (CTR Scientific, Monterrey, México), $C_7H_6O_5$ (Sigma Aldrich, St. Louis, MI, USA), NaOH (Jalmek Scientific, Nuevo León, México), 2-propanol, CAS: 67-63-0 (CTR Scientific, Chihuahua, Mexico). Potassium ferricyanide (CAS no.13746-66-2), potassium ferrocyanide (CAS no.14459-95-1), glucose (CAS no. 50-99-7), and fructose (CAS Number: 57-48-7) were purchased from Sigma-Aldrich (St. Louis, MI, USA). Potassium nitrate (CAS no. 7757-79-1), ascorbic acid (CAS no. 50-81-7), and fructose (CAS no. 57-48-7) were obtained from Golden Bell (Ciudad de Mexico, Mexico). Silver nitrate (CAS no. 7761-88-8) was acquired from Química Meyer (Ciudad de Mexico, Mexico). Potassium hydroxide (CAS no. 1310-58-3) was purchased from Fermont (Nuevo León, Mexico). During the procedures, all solutions were prepared with tridistilled water. Lithium hydroxide (LiOH), niobium ethoxide ($Nb(OCH_2CH_3)_5$), polyvinylpyrrolidone (PVP), acetic acid (CH_3COOH), and ethanol (C_2H_5OH) purchased from Sigma-Aldrich

(St. Louis, MI, USA). The counter electrode (CE ET055-1) was purchased from EDAQ (Colorado Springs, CO, USA), and a reference Ag/AgCl electrode (RE-1CP) was obtained from ALS Co., Ltd. (Tokyo, Japan).

2.2. Methods and Characterization

2.2.1. Silver Nanoparticle Synthesis

Silver nanoparticles were synthesized as follows: first, 100 mL of a 0.01 M silver nitrate ($AgNO_3$) solution was prepared; then 0.1 g of gallic acid ($C_7H_6O_5$) dissolved in 10 mL of deionized water was added. Finally, the pH was adjusted to 10 using a 1.0 M sodium hydroxide (NaOH) solution. This methodology uses gallic acid as an oxidizing agent and colloid protector.

2.2.2. Lithium Niobate Perovskite Synthesis

LNB nanofibers were produced by electrospinning. To produce the nanofibers, a precursor solution consisting of lithium hydroxide (LiOH), niobium ethoxide ($Nb(OCH_2CH_3)_5$), and polyvinylpyrrolidone (PVP) dissolved in acetic acid (CH_3COOH) and ethanol (C_2H_5OH) was prepared. The molar composition of the starting solution was defined as $LiOH:Nb(OCH_2CH_3)_5$: $PVP:CH_3COOH:C_2H_5OH$, equivalent to 1:1:0.75:8.06:26.15, with the molar ratio of PVP determined for the monomer.

The procedure involved the preparation of solution A by dissolving 0.498 g of PVP in 10 mL of ethanol and stirring magnetically for 90 min at 350 rpm and 32 °C. Solution B was prepared by dissolving 3 mL of ethanol and 10 mL of acetic acid, then adding 0.155 g of lithium hydroxide followed by 1.7 mL of niobium ethoxide in a controlled atmosphere and stirring for 90 min at 350 rpm and 32 °C. Afterward, solution B was poured into solution A, and the resulting solution C was stirred for 14 h at 350 rpm and 32 °C. Solution C was then loaded into a syringe connected to the electrospinning equipment (NEU-Pro, NaBond Technologies Co., Ltd., Shenzhen, China) under a flow rate of 0.2 mL/h. To generate a potential difference, the applied voltages between the needle tip and collector were +17 KV and −8 KV, with a 15 cm distance between the needle tip and the collector. The equipment operated for approximately 12 h, needing periodic monitoring to ensure successful composite collection. Subsequently, the composite fiber was scraped off the aluminum and prepared for characterization.

The calcination of polymeric fiber was carried out by a tube furnace (21100, Thermolyne, Waltham, MA, USA) using alumina boats on a quartz tube and applying a 3 °C/min ramp for 2 h at 700 °C without a cooling ramp.

2.2.3. Pencil Electrode Preparation and Modification

A 5 cm long and 1.3 mm diameter graphite pencil lead (HB, Paper Mate, Oak Brook, IL, USA) was used as a conductive substrate for the homemade electrode assembly. It was then attached to a copper wire, which served as the electrode's contact. Copper conductive adhesive tape was used to attach the graphite tip to a 0.8 mm diameter copper wire, ensuring uniform contact between the two parts. An epoxy resin was then prepared and used to fix the pencil tip tied to the copper wire inside the body of a 3 mm diameter plastic syringe. Figure S1 (Supplementary Material) illustrates the electrode assembly. Before each use, the electrode surface was polished with 2000-grit sandpaper and a microfiber cloth. Then the pencil-side electrode tip was dipped into a container with deionized water and sonicated for 5 min. Afterwards, the electrode tip was polished again with the cloth, and the sample was deposited for analysis.

A perovskite suspension of 4 mg/mL was prepared for electrode surface modification. The silver nanoparticle solution was obtained from the reaction without any purification procedure. Various ratios of LNB:AgNP (1:1, 1:2, 1:4, 2:1, and 4:1) were formulated by mixing specific volumes of the previously prepared perovskite suspension and the product of the nanoparticle's synthesis. Volume ratios of each component are specified in Table 1. Subsequently, the mixtures were subjected to sonication for 3 min to obtain homogeneous

dispersions. In total, 8 µL of the 1:1, 1:2, 1:4, 2:1, and 4:1 mixtures were drop-casted on the electrode surface and left to dry for 30 min at room temperature. A nomenclature was established for the mixtures according to their corresponding LNB:AgNP ratio as LNB1:1AgNP, LNB1:2AgNP, LNB1:4AgNP, LNB2:1AgNP, and LNB4:1AgNP to denote ratios of LNB:AgNP of 1:1, 1:2, 1:4, 2:1, and 4:1, respectively.

Table 1. Compositions of evaluated LNB:AgNP ratios.

LNB:AgNP	Perovskite Volume (µL)	AgNP Volume (µL)
4:1	480	120
2:1	400	200
1:1	300	300
1:2	200	400
1:4	120	480

4:1, 2:1, 1:1, 1:2, and 1:4 correspond to volume ratio of each component.

2.2.4. Characterization Techniques

Electrospun and calcined perovskite fiber samples were deposited on carbon tape and placed in an aluminum sample holder for scanning electron microscopy characterization (SU3500, Hitachi, Tokyo, Japan). Operation conditions were 5.00 kV, vacuum, and working distance of 6.5 mm. The images were obtained using backscattered electron detectors. In addition, a transmission electron microscope (HT7700, Hitachi, Tokyo, Japan) operating at 100.0 kV was used to complement perovskite characterization. Samples were deposited onto carbon-membrane copper grids. The solvent was allowed to evaporate at 30 °C for 30 min. An X-ray diffractometer (X'Pert PRO RX04, Malvern Panalytical, Worcestershire, UK) with Cu Kα1 radiation (1.540598 Å) was used to determine the crystalline structure of the lithium niobate perovskite. The nanofiber was isolated from the aluminum foil and applied onto a glass slide to produce a concentrated film. The analysis conditions were a scanning rate of 0.08° per s over a 2θ range from 10° to 90°.

A high-resolution transmission electron microscope (JEM-2200FS, Hitachi, Tokyo, Japan) in STEM mode was employed for silver nanoparticle morphology characterization. For the sample preparation, two drops of AgNP–isopropyl alcohol dispersion were placed onto a carbon-membrane copper grid.

Electrochemical characterization was carried out using a three-electrode cell. The arrangement of electrodes included a homemade electrode (ø = 1.3 mm), a platinum plate of 1 cm^2, and a Ag/AgCl that were used as the working electrode, counter electrode, and reference electrode, respectively. Cyclic voltammetry (CV), linear sweep voltammetry (LSV), and chronoamperometry techniques were performed using a potentiostat (Modular Admiral Instrument, Squidstat Prime, Eindhoven, The Netherlands). Cyclic voltammetry (CV) was evaluated at a potential window from −0.4 to 1.0 V and a scan rate of 100 mV s^{-1} during 3 oxidation-reduction cycles. The amperometry test was carried out to evaluate the ratio that evidenced optimum performance. The applied potential was 0.7 V, using a glucose concentration from 0 to 16 mM. Additionally, linear sweep voltammetry was employed to evaluate the selected LNB:AgNPs of optimum performance composites and investigate the response to a linear sweep of potential at a constant scan rate of 100 mV s^{-1}. The quantitative analysis of glucose was carried out using a 0.1 M sodium hydroxide (NaOH) solution (pH 13) as the supporting electrolyte. Linear sweep voltammetry was performed with glucose concentrations ranging from 0 to 8 mM, within a potential window of 0.4 to 1.0 V at a scan rate of 100 mV s^{-1}. The amperometric response of LNB/AgNP composites in the presence of glucose was measured by applying a constant potential of 0.7 V. Initially, the current was allowed to stabilize for 3 min with the blank solution (electrolyte without glucose). Then a standard solution (200 mM) was added incrementally to increase the glucose concentration by 1 mM with each addition. This process was repeated until the desired final concentration was reached. The measurements were taken with magnetic stirring at 600 rpm. A calibration curve was constructed based on three amperometric

readings. The same graphite pencil lead electrode was used throughout the experiment to minimize variations due to the electrode.

3. Results and Discussion

3.1. Silver Nanoparticle Characterization

Figure 1a illustrates the morphology of the silver nanoparticles used as the electrocatalyst. As seen, the particles are semispherical with diameters close to 10 nm. During HRTEM analysis, it was observed that mostly the nanoparticles are occluded within droplets of the colloid protective agent. In the magnification, Figure 1b, the geometry of the silver nanoparticles and even the crystalline planes are observed. A mapping of elements was carried out to complement the characterization. In Figure 1c,d, the area covered by the grid used as the support and the shell of the colloid protector is seen in red, indicating its organic character. Furthermore, in cyan the area corresponding to silver is observed, demonstrating the composition of the nanoparticles.
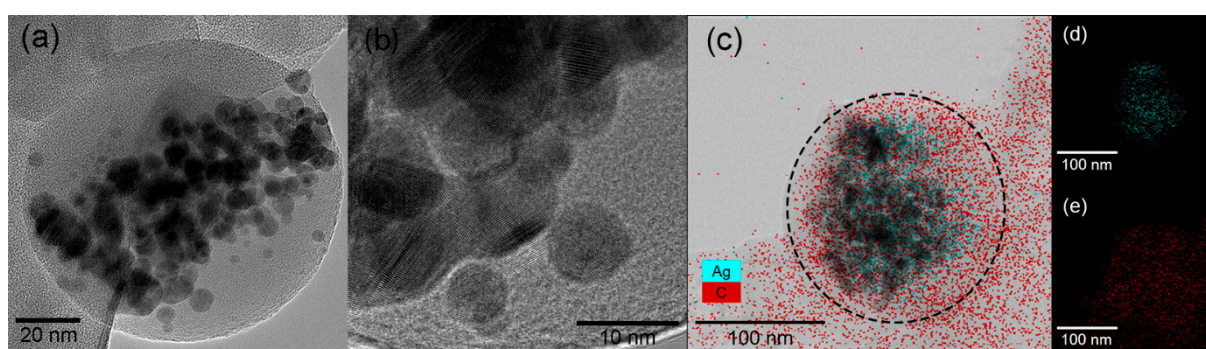

Figure 1. (**a**,**b**) TEM images of silver nanoparticles at low and high magnification. Encapsulation of the nanoparticles by the colloidal stabilizer (gallic acid) is observed. (**c**–**e**) Elemental mapping. The carbon in the organic components is observed in red and the silver in the nanoparticles in blue.

Dynamic light scattering (DLS) analysis was performed to determine particle size and complement the morphological analysis of the AgNPs. An average particle size of 11.4 nm was determined, with a standard deviation of ±6.6 nm. The particle size determined by this technique agrees with that observed in the TEM images. The zeta potential showed a negative electrical charge of −35.0 mV, with a dispersion of ±3.3 mV. This result indicates a low agglomeration risk of the nanoparticles.

3.2. Perovskite Characterization

Structural and Morphological Characterization

Figure 2 displays the X-ray diffraction (XRD) pattern of the obtained electrospun fiber and perovskite after thermal treatment. As observed, the electrospun fibers show a wide band centered in 2θ of 27.3°; this kind of diffraction pattern is characteristic of amorphous polymers, in this case, polyvinylpyrrolidone.

As for the thermally treated material, the diffractogram exhibits a series of peaks. According to the indexation using the ICDD database released in 2010 with card number 00-074-2241, the pattern properly fits the crystallographic phase for lithium niobate. In addition, the spectrum indicates a rhombohedral-type space group for the LNB perovskite. Regarding the main peaks of the diffractogram, the 2θ position of 23.5° confirms the crystalline phase of LNB. This peak corresponds to the (012) plane; its high intensity suggests that this plane is well aligned with the X-ray beam direction, indicating a strong presence and good crystallization of this plane in the sample. The peak at 2θ of 33.5° corresponds to the (104) plane. The relative intensity of 45% compared to the first peak suggests that this plane is in smaller quantity or less aligned with the X-ray beam. However, its presence remains significant, indicating good crystallinity of this plane in the sample. Finally, the peak at 2θ of 35.0° corresponds to the (110) plane. The relative intensity of 29% is

the lowest among the three analyzed peaks, suggesting that this plane is present in smaller quantities or is less prominent in the sample. Despite its lower intensity, the presence of the peak at the expected 2θ position confirms the crystalline structure of LNB [20].
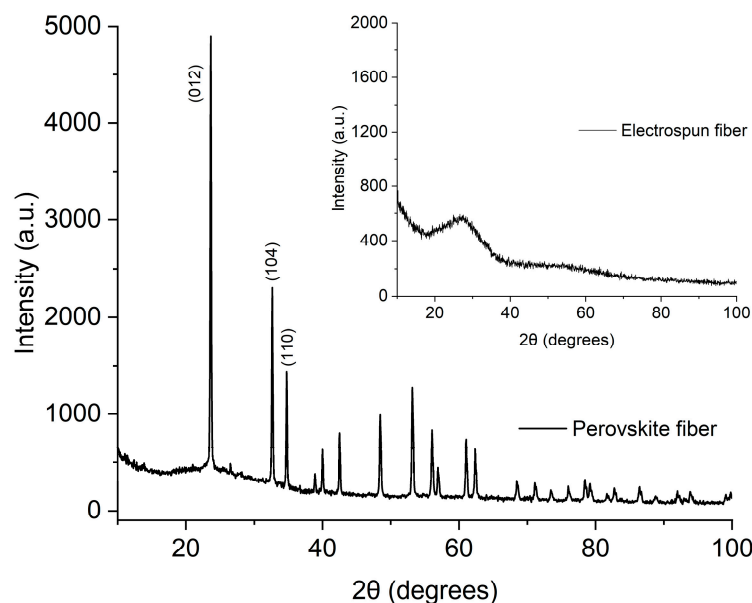

Figure 2. XRD pattern of the LiNbO$_3$ perovskite nanofiber and electrospun fiber (inset).

Figure 3a,b show the fibers obtained from the electrospinning process. As noted, the fibers form a web-like 3D mat of interconnected fibers with an average diameter size close to 500 nm and a narrow fiber diameter distribution. The necklace-like morphology exhibited by the nanofibers is characteristic of the electrospun compounds. After calcination, the fibers were once more analyzed by SEM, as seen in Figure 3c. It is observed that the smooth surface of the pristine fibers has been lost, which indicates the disappearance of the organic phase. After heat treatment, the perovskite displays a fibrous interconnected structure, apparently formed by the consecutive union of linked lobular substructures. Figure 3d provides a closer view of the LNB structure, where the segmented-interconnected structure with diameters ranging from 100 to 200 nm is observed. The reduction in diameter is due to the removal of polymer content, with approximately 50% of the mass representing the precursor. To delve deeper into the perovskite structure, transmission electron microscopy was performed. Figure 3e portrays the fibrous structure, with a slightly wide fiber diameter dispersion. A branched structure is also observed, where fibers emanate from a main trunk that is usually larger in diameter. The magnification, Figure 3f, shows clearly the segmented nature of the fiber, as commented before, where sequentially linked oval grains of about 100 nm wide are observed to form the fibers. It is worth noting that this behavior is not uniform across the sample, as various geometric shapes are also observed. The change in crystal morphology is attributed to adjustments in the applied voltage difference at the needle tip, slightly modifying the morphology of the spun fibers. For example, Gao et al. [21] demonstrated that the morphology of multi-wall Sn/SnO$_2$@carbon composite hollow nanofibers synthesized by electrospinning can be finely tuned by adjusting the precursor solution properties (such as polymer concentration and viscosity), the electrospinning parameters (voltage, flow rate, and collector distance), and the post-processing conditions (calcination temperature and time). By controlling these parameters, the researchers were able to transition between the formation of nanofibers and nanoparticles, providing valuable insights into the design and fabrication of nanostructures with specific properties tailored for various applications
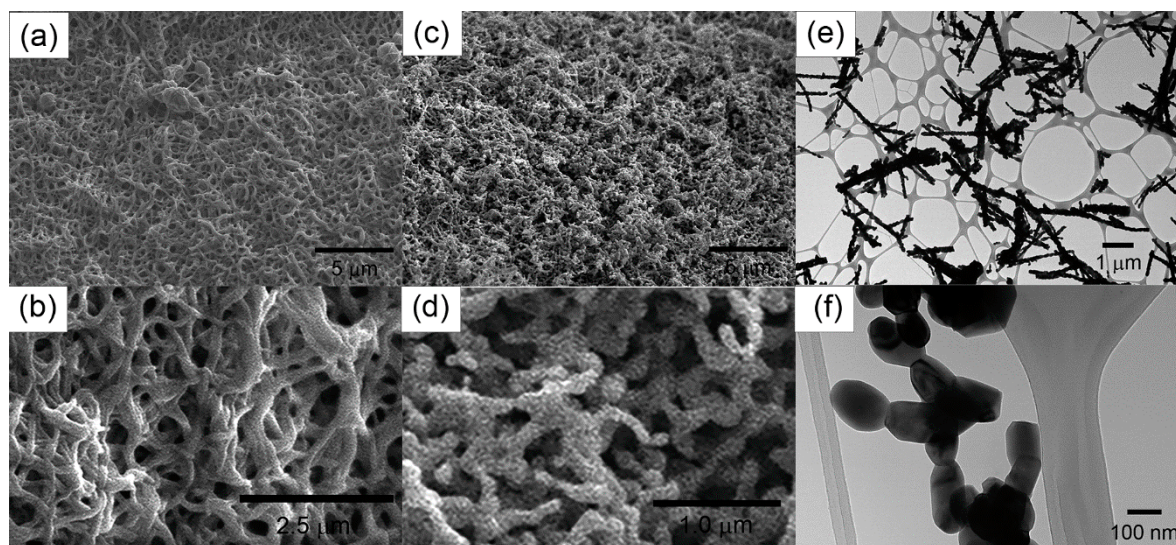
Figure 3. Morphology of lithium niobate fibers. (**a**,**b**) SEM images of the pristine fibers obtained from the electrospun process. (**c**,**d**) SEM images of the lithium niobate after the thermal treatment. (**e**,**f**) TEM images of the lithium niobate perovskite after thermal treatment. The applied voltage between the needle tip and collector during electrospinning was +17 kV to −8 kV.

3.3. LNB/AgNp Composite Characterization

3.3.1. Exploratory Analysis for Glucose Detection

Homemade electrode performance was evaluated by CV to demonstrate its correct operation using the redox pair $K_3[Fe(CN)_6]/K_4[Fe(CN)_6]$. The CV was conducted at a scan rate of 100 mV/s, and the electrode showed well-defined redox peaks with quasi-reversible behavior and a ΔEp of 150 mV (CV of the bare electrode is available in the Supporting Material (Figure S2).

Using a low-cost graphite pencil lead electrode for electrochemical glucose sensing offers several advantages over commercial electrodes, especially in terms of cost, accessibility, and customization. Commercial electrodes are expensive, particularly single-use ones (screen-printed electrodes). However, the electrode used in this research, in addition to allowing electrochemical analysis using various techniques, is perfectly reusable without losing its effectiveness and reproducibility, and the environmental impact associated with the production and disposal of electronic waste is reduced.

AgNPs have been widely used in designing glucose electrochemical sensors due to their intrinsic features, such as high electrical conductivity, surface area, catalytic activity, plasmonic properties, chemical stability, and ease of surface modification capacities [22,23]. Although AgNPs catalyze glucose oxidation, their use in nanocomposites enhances stability, improves selectivity, optimizes reaction kinetics, and optimizes cost-effectiveness relationships [24]. Perovskite-type nanomaterials have gained significant attention in the electrochemical detection of analytes, both as standalone materials and in the form of nanocomposites. Usually, perovskites exhibit low electroactivity, so they are combined with other materials (i.e., graphene and other carbon nanostructures) to overcome the limitations and enhance their electrochemical performance [25]. In this work, various LNB/AgNP ratios were studied to design an electrochemical glucose sensor. The LNB:AgNP ratios were 1:1, 1:2, 1:4, 2:1, and 4:1, identified as LNB1:1AgNP, LNB1:2AgNP, LNB1:4AgNP, LNB2:1AgNP, and LNB4:1AgNP, respectively, to correlate the ratio with the best responses in terms of glucose detection and stability of the electrochemical sensor.

Figure 4a shows the voltammograms of LNB/AgNP composites with and without glucose. The CV measurements employed a basic supporting electrolyte of 0.1 M NaOH (pH 13). In this medium, AgNps suffer from three oxidation reactions during the anodic scan. The signals appear at 0.26, 0.4, and 0.8 V, corresponding to the formation of AgOH,

Ag_2O, and AgO, respectively [26]. Then, during the cathodic sweep, the corresponding reduction reactions occurred, producing Ag_2O and Ag species on the electrode surface. These reactions occur at a potential of 0.4 and 0 V, respectively. Upon adding glucose at a concentration of 5 mM, a new evident signal appears at 0.7 V. This cathodic peak corresponds with the glucose oxidation [27]. The oxidation mechanism is as follows: First, the glucose molecules ($C_6H_{12}O_6$) adsorb onto the silver nanoparticles' surface, specifically at the region of the active Ag_2O species, which facilitates the oxidation reaction. Glucose adsorption is a crucial step as it allows direct interaction between glucose and the reactive surface of the nanoparticle. Glucose is oxidized on the surface to become gluconolactone ($C_6H_{10}O_6$), and electrons are transferred to the surface of silver nanoparticles (Equation (1)):

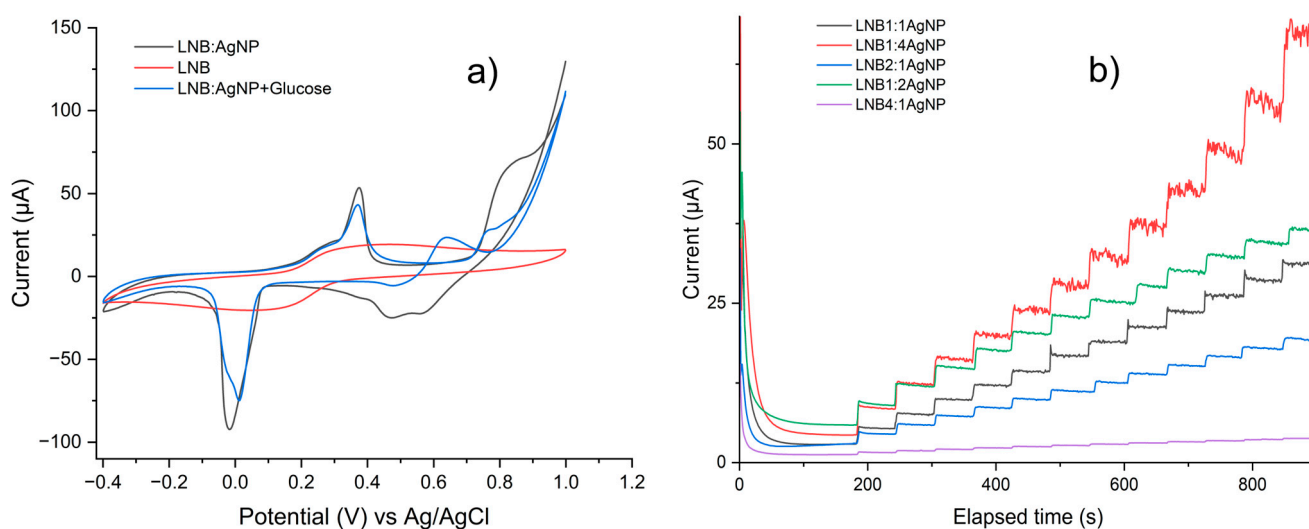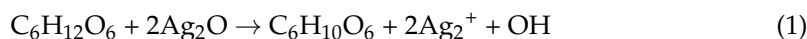$$C_6H_{12}O_6 + 2Ag_2O \rightarrow C_6H_{10}O_6 + 2Ag_2^+ + OH \tag{1}$$

Figure 4. Exploratory analysis of glucose. (**a**) Cyclic voltammograms of LNB, LNB:AgNP without glucose, and LNB:AgNP in the presence of 5 mM glucose. (**b**) Amperometric glucose detection of LNB1:1AgNP, LNB1:4AgNP, LNB2:1AgNP, LNB1:2AgNP, and LNB4:1AgNP.

In this process, species on the surface of the AgNps are reduced back to metallic silver (Ag), releasing electrons that are recorded as current at the electrode. After glucose oxidation, the silver nanoparticles are regenerated by reforming Ag_2O in the presence of OH^- from the basic medium. This cycle allows the silver nanoparticles to continue oxidizing glucose in the basic medium.

The study of the various LNB:AgNP ratios has provided significant insights into how the material composition influences sensor performance. The results from chronoamperometry clearly show a dependence of the electrochemical response on the silver content. Figure 4b indicates that a higher silver content in the sensor composition leads to a more pronounced increase in current with the addition of glucose. This is consistent with the fact that silver nanoparticles are well known for their excellent catalytic ability to oxidize glucose, which enhances electron transfer and, consequently, the amperometric signal. Specifically, the LNB1:4AgNP ratio, the one with the highest silver content, showed a significantly greater increase in current compared to the others, highlighting the dominant contribution of silver in catalyzing the reaction. However, a critical aspect was the measurement instability as the silver content increased even at low glucose concentrations (e.g., 4 mM). This behavior was attributed to the tendency of AgNPs to agglomerate when present in high concentrations. Under these conditions, although catalytically active, the nanoparticles lose efficiency due to poor dispersion. In addition, the agglomeration reduces the active area available for the glucose oxidation reaction and causes signal fluctuations due to the variability in local catalytic activity. Furthermore, the high concentration of

AgNPs may generate competition between the active silver sites, resulting in an elevated overpotential and decreasing sensor stability. Additionally, at high silver concentrations, there is a greater chance of side reactions or parasite currents, which contribute to a noisier signal during detection [28]. The increase in signal noise makes it more challenging to accurately quantify glucose, particularly at lower concentrations. As observed, as the perovskite content increased, the detection showed greater stability in measurements even upon greater glucose concentration, albeit with a less pronounced increase in current.

Based on the performance of the composite with the lowest AgNP ratio, considering cost optimization, improved stability and durability, reduced interferences, and selectivity, the LNB4:1AgNP composite was selected for further sensor design, as this approach allows taking advantage of the unique properties of both components in a balanced manner, maximizing sensor performance in practical applications.

3.3.2. Morphological Characterization and Electrochemical Performance of LNB4:1AgNP Composites

Figure 5 illustrates the morphology of the LNB4:1AgNP composite. In Figure 5a, the composite is shown at low magnification, revealing the fibrillar structure of the perovskite with AgNPs distributed on the surface of the fibers. Figure 5b,c present images at higher magnifications, where the particulate nature of the perovskite fibers is evident and the deposition of the silver nanoparticles on the fibers' surface is unmistakable, confirming the surface interaction between the components. Figure 5d–f show EDS mapping analysis, where homogeneous well-distributed silver nanoparticles over the perovskite surface can be observed. The relative concentration of the metals was 20.4 and 6.4 at% for Nb and Ag, respectively. The morphologies of the nanoparticles and the perovskite align with those observed in Figures 1 and 3, respectively. This observation is consistent with the previous amperometric measurements, where the good performance of the LNB4:1AgNP composite was partially attributed to the homogeneous distribution of the catalytic material.
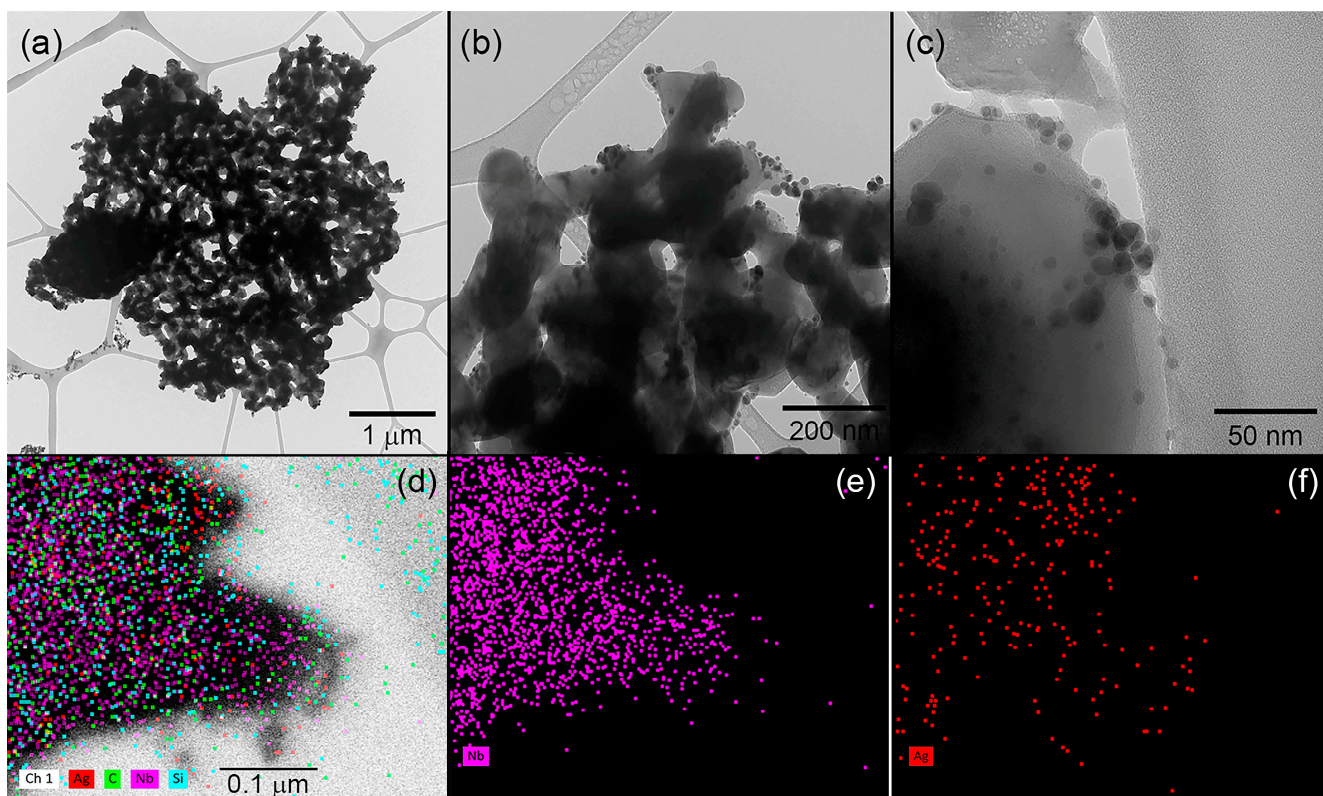

Figure 5. (**a**–**c**) TEM images of silver nanoparticles deposited on LNB perovskite nanofibers at various magnifications. (**d**–**f**) EDS mapping analysis of LNB4:1AgNP composite.

The linear sweep voltammetry (LSV), Figure 6a, emphasized the signal attributed to the glucose oxidation, appearing at 0.7 V. It was observed that LSV gives a good correlation of current against glucose concentration; however, it resulted in a limited linear range. The linear detection range of an electrochemical sensor refers to the analyte concentration at which the sensor response (current) is directly proportional to the analyte concentration. When using LSV for glucose quantification, it was observed that the sensor response was no longer linear at analyte concentrations exceeding 8 mM, as shown in Figure 6b. It is attributed to the complexities introduced by potential sweeping and competitive processes, for which the electrochemical technique often exhibits a narrower linear detection range. As the potential sweeps, the combination of kinetic factors, capacitive currents, and side reactions can cause the current response to deviate from a simple linear relationship with analyte concentration. Consequently, it is complex to maintain a consistent response over a broad range of concentrations.
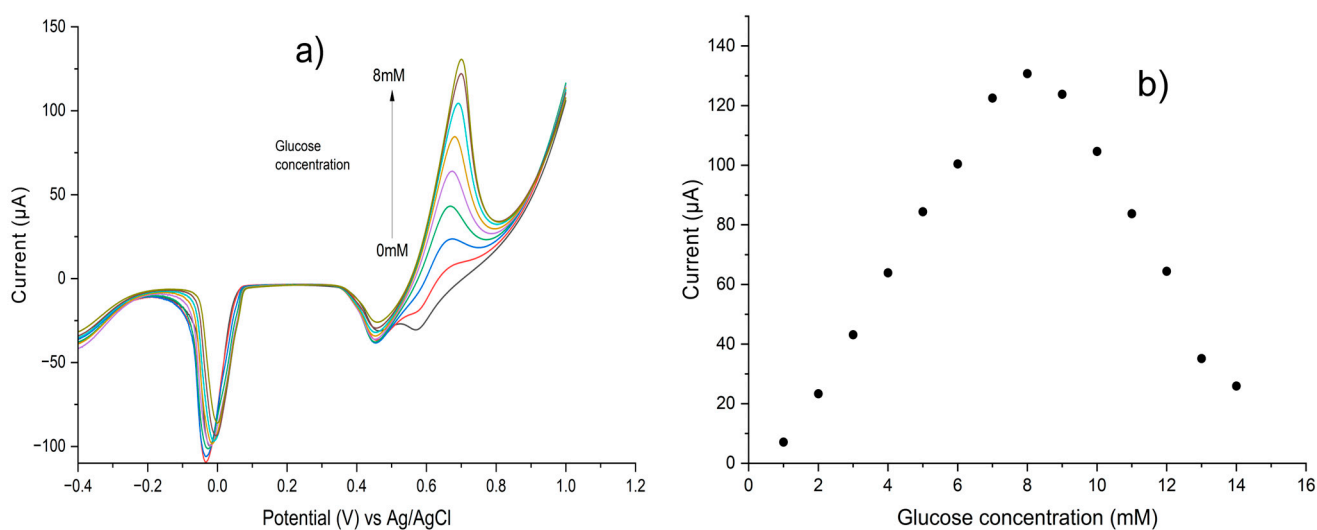

Figure 6. (**a**) Linear sweep voltammetry (LSV) of glucose concentration varying from 0 to 8 mM using LNB4:1AgNP electrode and 0.1 M NaOH electrolyte. (**b**) Calibration curve of glucose vs. current with glucose concentration varying from 0 to 14 mM. The tests were performed using the homemade electrode.

For application as a glucose-sensing device, such as a glucometer, the sensor should detect blood glucose concentrations within a range clinically relevant for diabetes monitoring. Therefore, a glucose-sensing device must accurately measure within these ranges, especially around critical diagnostic and control values such as 3 and 11 mM, to provide useful information for preventing and managing diabetes. Consequently, chronoamperometry was employed for the glucose quantification, aiming to avoid many of these complexities by holding the potential constant, allowing the reaction to reach a steady state. This steady-state condition minimizes the impact of capacitive currents and side reactions, resulting in a more direct and linear relationship between the current and analyte concentration over a broader range.

Figure 7a demonstrates that perovskite plays an important role in increasing the electrocatalytic activity of the AgNPs since the superior performance of the LNB:AgNP in glucose oxidation is evident, compared to the same amount of silver without the presence of perovskite. Furthermore, the resulting current response is much less noisy, making glucose detection simpler and with a much greater linear response range. It can be explained by several factors related to the synergistic properties that arise from both materials' combination, such as improved nanoparticle distribution, catalytic synergy, enhanced electron transfer, creation of new interfacial active surfaces, and improved material stability [29–31]. These combined effects lead to higher currents in chronoamperometry, indicating greater efficiency in glucose detection. Figure 7b displays the calibration curve obtained from

chronoamperometry for the LNB4:1AgNP composite. It shows the current vs. glucose concentration upon the injection of 1 mM of the analyte at a fixed potential of 0.7 V. The recorded data exhibited a linear range from 1 to 15 mM, a sensitivity of 0.2 µA/mM with a fitting of $R^2 = 0.997$, and a limit of detection (LOD) of 0.5 µM. The limit of detection (LOD) of the electrochemical glucose sensor was calculated using a methodology based on the standard deviation of the baseline (noise) signal and the slope of the calibration curve of Ipa vs $v^{\frac{1}{2}}$ [32].
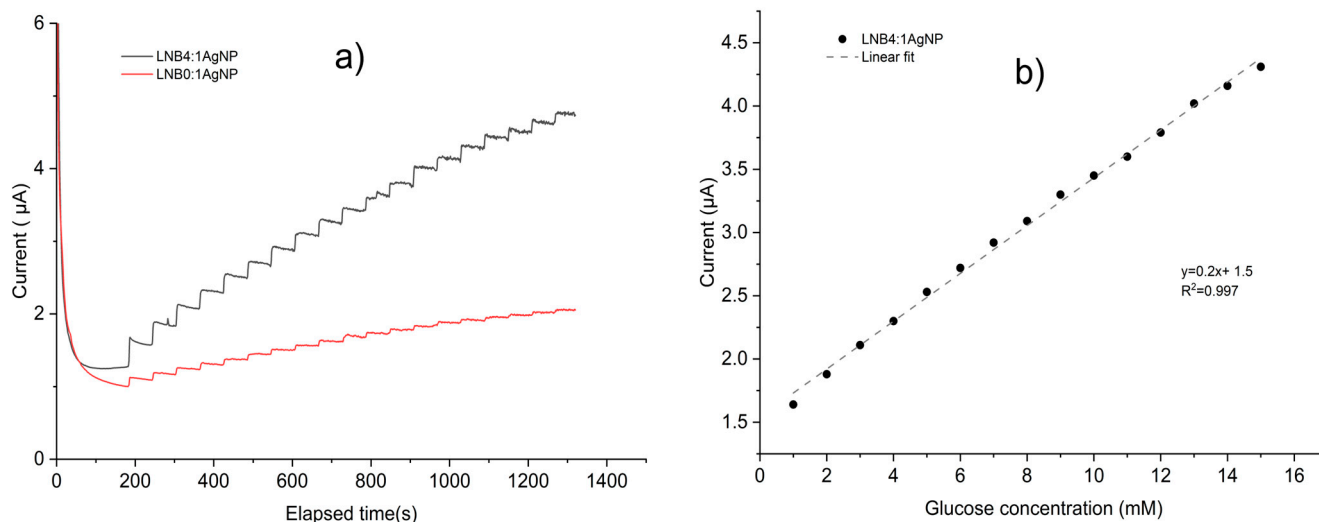

Figure 7. (**a**) Amperometric glucose detection using LNB4:1AgNP vs. the same content of AgNP without perovskite (LNB0:1AgNP). (**b**) Calibration curve of LNB4:1AgNP varying glucose concentration from 1 to 15 mM. The tests were performed using the homemade electrode.

The electroactive areas of AgNP, LNB, and LNB4:1AgNP were determined by cyclic voltammetry. The Randles–Sevick equation for a reversible redox reaction at room temperature (25 °C) is given by Equation (2):

$$I_{pa} = (2.69 \times 10^5) \times n^{\frac{3}{2}} \times AC \times \sqrt{Dv} \tag{2}$$

where I_{pa} stands for the anodic peak current (in amperes), *n* is the number of electrons transferred in the redox reaction (for ferrocyanide, *n* = 1), A is the electroactive area of the electrode (in cm^2), D is the diffusion coefficient of the redox species (for ferrocyanide, D = 7.6×10^{-6} at room temperature), C is the concentration of the redox species (in mol/cm^3, for 5 mM = 5×10^{-6} mol/cm^3), and *v* is the scan rate of the voltammetry experiment (in V/s). From Equation (2), A can be calculated from the slope of the I_{pa} vs. (scan rate)$^{1/2}$ plot, and then the value was used for the calculation. Cyclic voltammograms of LNB4:1AgNP, varying the scan rate from 10 to 100 mV/s, are shown in Figure 8, and the corresponding LNB and AgNP are also provided in Supplementary Material (Figure S3a,b). The calculated electroactive surface area of LNB, AgNP, and LNB4:1AgNP was 0.0046 cm^2, 0.0037 cm^2, and 0.0040 cm^2, respectively. This result shows the larger surface area of the nanofibers, although as seen in Figure 4a, they do not have enough electroactive behavior by themselves. Additionally, it is evident that LNB4:1AgNP offers significant advantages over silver nanoparticles used in individual ways. The improved electrochemical response of the nanocomposite was attributed to the AgNP's excellent electrical conductivity when combined with the perovskite, which may have low electrical conductivity but high adsorption capacity [33,34]. The resulting nanocomposite can exhibit enhanced conductivity, facilitating electron transfer during the glucose oxidation reaction. Consequently, the combination of both materials results in a higher density of active sites and faster reaction kinetics, improving the sensor sensitivity.
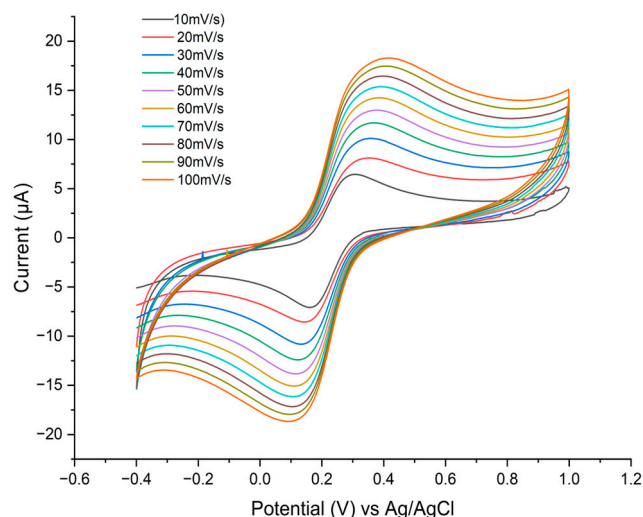
Figure 8. Cyclic voltammetry of LNB4:1AgNP, varying the scan rate from 10 to 100 mV/s.

3.3.3. Interference Test

In the context of electrochemical glucose sensors, it is essential to identify and manage interferents—substances that can oxidize or reduce at the electrode, generating signals that interfere with the accurate glucose measurement. The most common interferents in the blood include uric acid, ascorbic acid, and other sugars, such as fructose and sucrose [35–37]. Additionally, other components such as potassium chloride (KCl), sodium chloride (NaCl), and urea do not directly interfere with glucose detection in blood because these do not undergo redox reactions at the potentials typically used for glucose oxidation; however, they can still affect sensor performance. For instance, potassium ions (K^+) are crucial in maintaining blood ionic strength and conductivity, influencing the sensor's overall functionality [38]. Variations in KCl concentration, for example, alter the double-layer capacitance at the electrode interface, potentially leading to changes in background currents [39]. Consequently, the selectivity of LNB4:1AgNP was evaluated as shown in Figure 9. A known concentration of the interferents uric acid, ascorbic acid, fructose, KCl, and NaCl were injected during the amperometry test. The signal at 120 s of elapsed time corresponds to 1 mM glucose. Thus, after 60 s, the ascorbic acid solution was added to the electrolyte and, afterward, at 240, 300, 360, and 420 s, solutions of uric acid, KCl, NaCl, and fructose were added, respectively. Subsequently, at elapsed times of 480, 540, 600, 660, and 720 s, additions of glucose were introduced into the electrolyte. It should be noted that the addition of the different interferents did not register any response in the sensor detection. However, after successive additions of glucose, a decrease in the response current was recorded, demonstrating that part of this substance, which could be ions, partially blocks the surface of the electrode, reflecting that although the surface remains active, there was a slight loss of sensitivity.

To compare our results with other works that used perovskites-based composites even as support or electrocatalysts for the sensing of glucose or other interest analytes such as hydrogen peroxide or dopamine, we consider parameters such as LOD, sensitivity, and linear range (see Table 2). These are the most critical parameters for an electrochemical sensor. As observed, the results are quite similar in terms of sensitivity and LOD to other reported works, even when the used electrode here (homemade) does not have the same purity, structure, and conductivity of a commercial glassy carbon electrode. Additionally, our sensor can measure across an exceptionally wide range, spanning from normal levels to critical values associated with severe hyperglycemia. Conventional glucose sensors are typically designed to cover a standard range from 4 to 11 mM (72 to 200 mg/dL), corresponding to normal and slightly elevated physiological levels. This advancement is of great importance for monitoring patients with metabolic disorders, especially those with

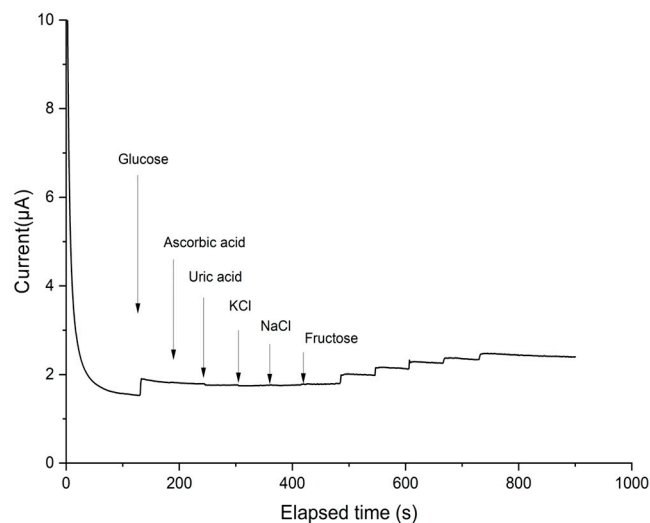chronic hyperglycemia or diabetes mellitus, where blood glucose levels can significantly exceed normal values.

Figure 9. Interference test evaluation using glucose (1 mM), potassium chloride (KCl 3.5 mM), sodium chloride (NaCl 135 mM), uric acid (0.2 mM), fructose (0.10 mM), and ascorbic acid (0.2 mM).

Table 2. Comparison of LNB/AgNP with other perovskite-based composites for non-enzymatic detection of analytes.

Perovskite-Based Material	LOD (μM)	LR (μM)	Sensitivity (μA/mMcm^2)	Analyte	Evaluated Interferents	Reference
LaSrCoO/GO	0.05 0.063	0.2–3350 2–3350	500 330	H_2O_2 Glucose	DA, UA, AA	[39]
NdFeO$_3$/glycine/CNTs	113.2	0.003–200	113.2	AML AA	UA, DA, EP, APAP	[40]
SrTiO$_3$/rGO	0.11–0.15	0.3–0.8	13.16–193.43	NA	Ph, Tol, Chloph, Cat, ChBz, etc.	[41]
LaTiO$_3$-Ag$_{0.1}$	0.0025	0.01–0.10	780	Glucose	Gly, Alni, Fru, Mal, UA, AA, etc.	[42]
LaTiO$_3$-Ag$_{0.2}$	0.21	2.5–4000	784.14	Glucose	DA, UA, AA	[43]
AuNPs/SrPdO$_3$	10.1	100–6000	-------	Glucose	DA, UA, AA, APAP, Chlor	[44]
LNB/AgNP	0.5	100–16,000	526	Glucose	UA, AA, KCl, NaCl, Fru	This work

EP = epinephrine, APAP = paracetamol, UA = uric acid, AA = ascorbic acid, DA = Dopamine, rGO = reduced graphene oxide, GO = graphene oxide, CNTs = carbon nanotubes, NA = nitroaromatics, Ph = phenol, Tol = toluene, Chloph = chlorophenol, Cat = catechol, ChBz = chlorobenzene, Gly = glycine, Alni = alanine, Fru = fructose, Mal = maltose, AuNp = gold nanoparticles, Chlor = chloride.

4. Conclusions

The research utilized 10 nm silver nanoparticles (AgNPs) as a catalyst to develop a non-enzymatic electrochemical sensor for glucose. While the AgNPs can detect the target analyte, adding a support material like perovskite resulted in a more stable measurement, even at high glucose concentrations. This was due to a significant increase in the electroactive area from 0.0037 cm^2 for AgNP alone to 0.0040 cm^2 for the LNB4:1AgNP composite. At high concentrations, the active nanoparticles tend to clump together, leading to non-uniform distribution on the electrode surface, reducing the area available for glucose oxidation and causing signal fluctuations. The sensor showed a detection range from 1 to 15 mM, covering the clinically relevant glucose concentration for detection devices.

This wide linear range is vital for diabetes monitoring, allowing accurate detection of blood glucose concentrations within critical diagnostic and control values (3 to 11 mM). Furthermore, the sensor showed no response to common interferents, like uric acid, ascorbic acid, or sugars; however, a slight decrease in sensitivity was observed with the addition of these substances, suggesting partial blockage of the electrode surface.

Supplementary Materials: The following supporting information can be downloaded at: https://www.mdpi.com/article/10.3390/chemosensors12100210/s1, Figure S1: Conformation of the homemade electrode; Figure S2: Cyclic voltammogram of homemade electrode. CV was conducted by $K_3[Fe(CN)_6]/K_4[Fe(CN)_6]$ redox probe and a scan rate of 100 mV/s; Figure S3a Cyclic voltammetry of LNB varying the scan rate from 10 to 100 mV/s obtained with 5 mM $K_3[Fe(CN)_6]/K_4[Fe(CN)_6]$; Figure S3b Cyclic voltammetry of AgNP varying the scan rate from 10 to 100 mV/s obtained with 5 mM $K_3[Fe(CN)_6]/K_4[Fe(CN)_6]$; Figure S3c Cyclic voltammetry of LNB4:1AgNP varying the scan rate from 10 to 100 mV/s obtained with 5 mM $K_3[Fe(CN)_6]/K_4[Fe(CN)_6]$.

Author Contributions: Conceptualization, C.I.P.-B. and E.A.Z.-C.; methodology, C.I.P.-B., A.M.-T., L.F.E.-C., S.Y.R.-L. and M.C.M.-O.; validation, C.I.P.-B., A.E-M. and C.A.H.-E.; formal analysis, C.I.P.-B., C.A.H.-E., L.F.E.-C. and S.Y.R.-L.; investigation, C.I.P.-B., A.M.-T. and M.C.M.-O.; data curation, C.I.P.-B. and C.A.H.-E.; writing—original draft preparation, C.I.P.-B., M.C.M.-O. and C.A.H.-E.; writing—review and editing, C.I.P.-B. and E.A.Z.-C.; supervision, E.A.Z.-C.; funding acquisition, E.A.Z.-C. All authors have read and agreed to the published version of the manuscript.

Conflicts of Interest: The authors declare no conflicts of interest.

References

1. Barhoum, A.; Hamimed, S.; Slimi, H.; Othmani, A.; Abdel-Haleem, F.M.; Bechelany, M. Modern Designs of Electrochemical Sensor Platforms for Environmental Analyses: Principles, Nanofabrication Opportunities, and Challenges. *Trends Environ. Anal. Chem.* **2023**, *38*, e00199. [CrossRef]

2. Mahmudiono, T.; Olegovich Bokov, D.; Abdalkareem Jasim, S.; Abdelbasset, W.K.; Dinora, M.K. State-of-the-Art of Convenient and Low-Cost Electrochemical Sensor for Food Contamination Detection: Technical and Analytical Overview. *Microchem. J.* **2022**, *179*, 107460. [CrossRef]

3. Reddy, K.K.; Bandal, H.; Satyanarayana, M.; Goud, K.Y.; Gobi, K.V.; Jayaramudu, T.; Amalraj, J.; Kim, H. Recent Trends in Electrochemical Sensors for Vital Biomedical Markers Using Hybrid Nanostructured Materials. *Adv. Sci.* **2020**, *7*, 1902980. [CrossRef] [PubMed]

4. Malhotra, S.; Tang, Y.; Varshney, P.K. Amperometric Enzyme-Free Glucose Sensor Based on Electrodeposition of Au Particles on Polyaniline Film Modified Pt Electrode. *Acta Chim. Slov.* **2018**, *65*, 687–697. [CrossRef]

5. Hayden, B.E. Particle Size and Support Effects in Electrocatalysis. *Acc Chem. Res.* **2013**, *46*, 1858–1866. [CrossRef]

6. Beaver, K.; Dantanarayana, A.; Minteer, S.D. Materials Approaches for Improving Electrochemical Sensor Performance. *J. Phys. Chem. B* **2021**, *125*, 11820–11834. [CrossRef]

7. Piñón-Balderrama, C.I.; Leyva-Porras, C.; Conejo-Dávila, A.S.; Estrada-Monje, A.; Maldonado-Orozco, M.C.; Reyes-López, S.Y.; Zaragoza-Contreras, E.A. Electrochemical Perovskite-Based Sensors for the Detection of Relevant Biomarkers for Human Kidney Health. *Chemosensors* **2023**, *11*, 507. [CrossRef]

8. Chakraborty, T.D.; Munmun, Y.L.; Chan, M.L.; Ray, H.K.; Chyuan. Highly Sensitive and Selective Detection of Diabetic Nephropathy Markers by a Perovskite $LaNiO_{3-x}$ Based Potentiometric Sensor. *J. Electrochem. Soc.* **2022**, *169*, 037507. [CrossRef]

9. He, J.; Sunarso, J.; Zhu, Y.; Zhong, Y.; Miao, J.; Zhou, W.; Shao, Z. High-Performance Non-Enzymatic Perovskite Sensor for Hydrogen Peroxide and Glucose Electrochemical Detection. *Sens. Actuators B Chem.* **2017**, *244*, 482–491. [CrossRef]

10. Atta, N.F.; Galal, A.; El-Ads, E.H. Effect of B-Site Doping on Sr_2PdO_3 Perovskite Catalyst Activity for Non-Enzymatic Determination of Glucose in Biological Fluids. *J. Electroanal. Chem.* **2019**, *852*, 113523. [CrossRef]

11. Sato, N.; Haruta, M.; Sasagawa, K.; Ohta, J.; Jongprateep, O. Fe and Co-Doped $(Ba, Ca)TiO_3$ Perovskite as Potential Electrocatalysts for Glutamate Sensing. *Eng. J.* **2019**, *23*, 265–278. [CrossRef]

12. Mahmoudi-Moghaddam, H.; Amiri, M.; Javar, H.A.; Yousif, Q.A.; Salavati-Niasari, M. A Facile Green Synthesis of a Perovskite-Type Nanocomposite Using Crataegus and Walnut Leaf for Electrochemical Determination of Morphine. *Anal. Chim. Acta* **2022**, *1203*, 339691. [CrossRef] [PubMed]

13. Atta, N.F.; Ali, S.M.; El-Ads, E.H.; Galal, A. Nano-Perovskite Carbon Paste Composite Electrode for the Simultaneous Determination of Dopamine, Ascorbic Acid and Uric Acid. *Electrochim. Acta* **2014**, *128*, 16–24. [CrossRef]

14. Chakraborty, T.; Das, M.; Lin, C.Y.; Lei, K.F.; Kao, C.H. Highly Sensitive and Selective Electrochemical Detection of Lipocalin 2 by NiO Nanoparticles/Perovskite CeCuOx Based Immunosensor to Diagnose Renal Failure. *Anal. Chim. Acta* **2022**, *1205*, 339754. [CrossRef]

15. Govindasamy, M.; Wang, S.F.; Pan, W.C.; Subramanian, B.; Ramalingam, R.J.; Al-lohedan, H. Facile Sonochemical Synthesis of Perovskite-Type SrTiO₃ Nanocubes with Reduced Graphene Oxide Nanocatalyst for an Enhanced Electrochemical Detection of α-Amino Acid (Tryptophan). *Ultrason. Sonochem* **2019**, *56*, 193–199. [CrossRef]

16. Atta, N.F.; Galal, A.; El-Gohary, A.R.M. Gold-Doped Nano-Perovskite-Decorated Carbon Nanotubes for Electrochemical Sensing of Hazardous Hydrazine with Application in Wastewater Sample. *Sens. Actuators B Chem.* **2021**, *327*, 128879. [CrossRef]

17. Chen, T.W.; Ramachandran, R.; Chen, S.M.; Anushya, G.; Rani, S.D.; Mariyappan, V.; Elumalai, P.; Vasimalai, N. High-performance-based Perovskite-supported Nanocomposite for the Development of Green Energy Device Applications: An Overview. *Nanomaterials* **2021**, *11*, 1006. [CrossRef]

18. Mazzotta, E.; Di Giulio, T.; Malitesta, C. Electrochemical Sensing of Macromolecules Based on Molecularly Imprinted Polymers: Challenges, Successful Strategies, and Opportunities. *Anal. Bioanal. Chem.* **2022**, *414*, 5165–5200. [CrossRef]

19. Ensafi, A.A.; Ahmadi, N.; Rezaei, B. Nickel Nanoparticles Supported on Porous Silicon Flour, Application as a Non-Enzymatic Electrochemical Glucose Sensor. *Sens. Actuators B Chem.* **2017**, *239*, 807–815. [CrossRef]

20. Chen, K.; Zhu, Y.; Liu, Z.; Xue, D. State of the Art in Crystallization of Linbo3 and Their Applications. *Molecules* **2021**, *26*, 7044. [CrossRef]

21. Gao, S.; Wang, N.; Li, S.; Li, D.; Cui, Z.; Yue, G.; Liu, J.; Zhao, X.; Jiang, L.; Zhao, Y. A Multi-Wall Sn/SnO₂@Carbon Hollow Nanofiber Anode Material for High-Rate and Long-Life Lithium-Ion Batteries. *Angew. Chem.-Int. Ed.* **2020**, *59*, 2465–2472. [CrossRef]

22. Sharma, V.K.; Yngard, R.A.; Lin, Y. Silver Nanoparticles: Green Synthesis and Their Antimicrobial Activities. *Adv. Colloid. Interface Sci.* **2009**, *145*, 83–96. [CrossRef]

23. Chen, X.; Schluesener, H.J. Nanosilver: A Nanoproduct in Medical Application. *Toxicol. Lett.* **2008**, *176*, 1–12. [CrossRef] [PubMed]

24. Saha, T.; Del Caño, R.; Mahato, K.; De la Paz, E.; Chen, C.; Ding, S.; Yin, L.; Wang, J. Wearable Electrochemical Glucose Sensors in Diabetes Management: A Comprehensive Review. *Chem. Rev.* **2023**, *123*, 7854–7889. [CrossRef]

25. Chen, T.W.; Ramachandran, R.; Chen, S.M.; Anushya, G.; Ramachandran, K. Graphene and Perovskite-Based Nanocomposite for Both Electrochemical and Gas Sensor Applications: An Overview. *Sensors* **2020**, *20*, 6755. [CrossRef]

26. Aparicio-Martínez, E.P.; Vega-Rios, A.; Osuna, V.; Dominguez, R.B. Salivary Glucose Detection with Laser Induced Graphene/AgNPs Non-Enzymatic Sensor. *Biosensors* **2023**, *13*, 207. [CrossRef]

27. Quan, H.; Park, S.U.; Park, J. Electrochemical Oxidation of Glucose on Silver Nanoparticle-Modified Composite Electrodes. *Electrochim. Acta* **2010**, *55*, 2232–2237. [CrossRef]

28. Ivanišević, I. The Role of Silver Nanoparticles in Electrochemical Sensors for Aquatic Environmental Analysis. *Sensors* **2023**, *23*, 3692. [CrossRef]

29. Noman, M.; Khan, Z.; Jan, S.T. A Comprehensive Review on the Advancements and Challenges in Perovskite Solar Cell Technology. *RSC Adv.* **2024**, *14*, 5085–5131. [CrossRef]

30. Li, Q.; Zhang, Y.; Zhang, G.; Wang, Y.; Pang, H. Recent Advances in the Development of Perovskite@metal-Organic Frameworks Composites. *Natl. Sci. Open* **2023**, *2*, 20220065. [CrossRef]

31. Saleh, H.M.; Hassan, A.I. Synthesis and Characterization of Nanomaterials for Application in Cost-Effective Electrochemical Devices. *Sustainability* **2023**, *15*, 10891. [CrossRef]

32. Shrivastava, A.; Gupta, V. Methods for the Determination of Limit of Detection and Limit of Quantitation of the Analytical Methods. *Chron. Young Sci.* **2011**, *2*, 21. [CrossRef]

33. Mokhtar, N.A.I.M.; Zawawi, R.M.; Khairul, W.M.; Yusof, N.A. Electrochemical and Optical Sensors Made of Composites of Metal–Organic Frameworks and Carbon-Based Materials. A Review. *Environ. Chem. Lett.* **2022**, *20*, 3099–3131. [CrossRef]

34. George, J.; Halali, V.V.; Sanjayan, C.G.; Suvina, V.; Sakar, M.; Balakrishna, R.G. Perovskite Nanomaterials as Optical and Electrochemical Sensors. *Inorg. Chem. Front.* **2020**, *7*, 2702–2725. [CrossRef]

35. Olejnik, A.; Karczewski, J.; Dołęga, A.; Siuzdak, K.; Grochowska, K. Novel Approach to Interference Analysis of Glucose Sensing Materials Coated with Nafion. *Bioelectrochemistry* **2020**, *135*, 107575. [CrossRef]

36. Xia, Y.; Huang, W.; Zheng, J.; Niu, Z.; Li, Z. Nonenzymatic Amperometric Response of Glucose on a Nanoporous Gold Film Electrode Fabricated by a Rapid and Simple Electrochemical Method. *Biosens. Bioelectron.* **2011**, *26*, 3555–3561. [CrossRef]

37. Mei, H.; Wu, W.; Yu, B.; Li, Y.; Wu, H.; Wang, S.; Xia, Q. Non-Enzymatic Sensing of Glucose at Neutral PH Values Using a Glassy Carbon Electrode Modified with Carbon Supported Co@Pt Core-Shell Nanoparticles. *Microchim. Acta* **2015**, *182*, 1869–1875. [CrossRef]

38. Huang, W.; Diallo, A.K.; Dailey, J.L.; Besar, K.; Katz, H.E. Electrochemical Processes and Mechanistic Aspects of Field-Effect Sensors for Biomolecules. *J. Mater. Chem. C Mater.* **2015**, *3*, 6445–6470. [CrossRef]

39. Hay, R.W. *Reaction Mechanisms of Metal Complexes*, 1st, ed.; Elsevier: Amsterdam, The Netherlands, 2000; ISBN 1-898563-41-1.

40. Atta, N.F.; El-Ads, E.H.; Galal, A.; Galal, A.E. Electrochemical Sensing Platform Based on Nano-Perovskite/Glycine/Carbon Composite for Amlodipine and Ascorbic Acid Drugs. *Electroanalysis* **2019**, *31*, 448–460. [CrossRef]

41. Ahmad, K.; Mohammad, A.; Mathur, P.; Mobin, S.M. Preparation of $SrTiO_3$ Perovskite Decorated RGO and Electrochemical Detection of Nitroaromatics. *Electrochim. Acta* **2016**, *215*, 435–446. [CrossRef]

42. Jia, F.F.; Zhong, H.; Zhang, W.G.; Li, X.R.; Wang, G.Y.; Song, J.; Cheng, Z.P.; Yin, J.Z.; Guo, L.P. A Novel Nonenzymatic ECL Glucose Sensor Based on Perovskite $LaTiO_3$-Ag0.1 Nanomaterials. *Sens. Actuators B Chem.* **2015**, *212*, 174–182. [CrossRef]

43. Wang, Y.Z.; Zhong, H.; Li, X.M.; Jia, F.F.; Shi, Y.X.; Zhang, W.G.; Cheng, Z.P.; Zhang, L.L.; Wang, J.K. Perovskite $LaTiO_3$-Ag0.2 Nanomaterials for Nonenzymatic Glucose Sensor with High Performance. *Biosens. Bioelectron.* **2013**, *48*, 56–60. [CrossRef] [PubMed]

44. El-Ads, E.H.; Galal, A.; Atta, N.F. Electrochemistry of Glucose at Gold Nanoparticles Modified Graphite/$SrPdO_3$ Electrode-Towards a Novel Non-Enzymatic Glucose Sensor. *J. Electroanal. Chem.* **2015**, *749*, 42–52. [CrossRef]